

Phase composition of regional seismic waves from underground nuclear explosions

Tae-Kyung Hong and Jiakang Xie

Lamont-Doherty Earth Observatory of Columbia University, Palisades, New York, USA

Received 31 March 2005; revised 10 August 2005; accepted 19 September 2005; published 7 December 2005.

[1] The mechanism of regional shear wave excitation by underground nuclear explosions (UNE), a long-standing issue in nuclear seismology, is investigated by studying the phase composition of regional waves from clustered UNE. Regional seismic waves from 67 UNE at the Balapan test site of Kazakhstan, recorded at station Borovoye, are analyzed with a source array technique under the reciprocity theorem. This analysis allows one to obtain the phase velocity composition of the plane waves leaving the source region. Source locations and the original times are obtained from geodetic measurements, a scaling law between event magnitude and depth, and a calibrated Pn travel time curve. Between frequencies of 0.5 and 3.0 Hz the Pn slowness power spectra are concentrated at a phase velocity (v_h) of 8.0 km/s. The expected Sn window contains two dominant phases: a scattered P wave with a v_h of around 7.1 km/s and a mantle shear wave with a v_h of 4.8 km/s. The Lg waves are coherent between 0.5 and 2.0 Hz, with a dominant v_h of 4.2 km/s, which is typical in SmS -type waves. The Rg wave at frequencies between 0.5 and 0.8 Hz is dominantly composed of a coherent fundamental mode Rayleigh wave with a v_h of 3.0 km/s. At higher frequencies (>0.8 Hz) this coherent Rayleigh wave is not observed in the Rg window because of attenuation during wave propagation. The slower v_h of Rg and faster v_h of Lg , at which the strong coherent peaks in slowness power spectra are observed, suggest that the dominant components of these two waves are different and they are originated differently in the source region. The proposed Rg -to- S scattering does not appear to be a dominant mechanism for Lg excitation in the Balapan test site. It is also found that the strength of shear waves contained in the expected Sn window varies with local geology much more than the strength of Lg does. Since the Sn is enriched in high-frequency (>1 Hz) content as compared to the Lg , this observation suggests that the local geology influences shear wave excitation at high frequencies more than at lower frequencies.

Citation: Hong, T.-K., and J. Xie (2005), Phase composition of regional seismic waves from underground nuclear explosions, *J. Geophys. Res.*, 110, B12302, doi:10.1029/2005JB003753.

1. Introduction

[2] There is a long-standing question on how regional shear waves, such as Sn and Lg waves, are generated by underground nuclear explosions (UNE). In the past decades, several mechanisms have been proposed for the regional shear wave excitation, such as spalling [Day and McLaughlin, 1991], Rg -to- S scattering [Gupta et al., 1992; Patton and Taylor, 1995; Myers et al., 1999], nonspherical S^* excitation [Gutowski et al., 1984; Vogfjörð, 1997], rock cracking [Massé, 1981], and tectonic release [Wallace et al., 1985].

[3] It has been difficult to evaluate the contribution of each proposed mechanism to the regional shear wave excitation [e.g., Xie and Lay, 1994]. Studies of waveforms recorded at regional distances typically suffer from an uncertainty about how the waveforms are affected by along-path propagation complications, such as three-dimensional scattering, after

they leave the source region and before they are recorded at the regional distances. It is not practical to deploy seismometers buried in the source zone to record the downgoing wave field that eventually evolves into regional waves.

[4] One way to study the composition of wavelets leaving the UNE sources is to use source array analysis by virtue of the reciprocity theorem. Hundreds of historic UNE were recorded by individual seismic stations at regional distances. Many explosions were clustered in small areas of the test sites with narrow ranges of depth variations. One particularly valuable data set is that from the Borovoye (BRV) historic seismogram archive [Kim et al., 2001] that recorded many UNE in the Balapan test site of Kazakhstan.

[5] Under the reciprocity theorem [Aki and Richards, 1980], velocity seismograms from these clustered explosion sources can be treated as seismograms at an array of fictitious strain meters buried at the source locations, recording a single force acting at the station location [Spudich and Bostwick, 1987; Xie et al., 1996; Nowack and Chen, 1999]. Source array techniques have been

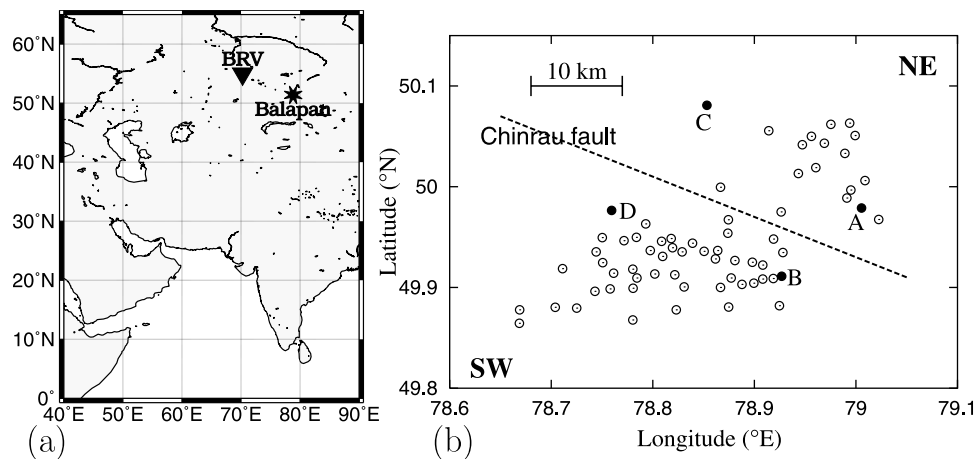


Figure 1. Maps showing locations of (a) the Borovoye observatory (BRV) and the Balapan nuclear test site and (b) locations of nuclear explosions in the test site. The explosion sources can be grouped into NE (18 events) and SW (49 events) subregions according to the velocity and geological structure. The dashed line dividing the Balapan region approximately delineates the Chinrau fault. Time records from four representative events (A, B, C, D) are given in Figure 10.

applied in various seismic studies [e.g., *Spudich and Bostwick*, 1987; *Gupta et al.*, 1990; *Scherbaum et al.*, 1991; *Xie et al.*, 1996]. In this study we apply a frequency–wave number (F-K) analysis technique to the source array seismograms and investigate the phase composition of regional waves recorded at BRV as they leave the source region.

2. Data and Local Geology

[6] The data used in this study are composed of short-period vertical seismograms from the Borovoye Observatory (BRV) in Kazakhstan of 67 UNE in the Balapan nuclear test site (Figure 1) recorded between 1968 and 1989. Data from two slightly different recording systems are used, both digitizing analog signals from sensor-type SKM-3 [*Kim et al.*, 2001]. The sampling interval is 0.032 s for one system (channel “sZ01”) and 0.096 s for the other (channel “s06Z”). Both systems have nearly flat peak displacement responses between about 1 and several hertz and recorded regional waveforms with high signal-to-noise ratios ($S/N > 50$ dB) between 0.5 and several hertz. The epicentral distances involved vary between 680 and 697 km (Figure 2).

[7] The event magnitudes (m_b) are between 4.8 and 6.2, with 58 out of the total 67 events having magnitudes larger than 5.5 [*Marshall et al.*, 1985; *Kim et al.*, 2001]. Precise hypocentral locations of the UNE are measured geodetically, with uncertainties of less than 200 m [*National Nuclear Centre of the Republic of Kazakhstan*, 1999; *Thurber et al.*, 2001]. Precise “ground truth” origin times and depths of burial are available for 10 UNE between 1985 and 1989 [*Adushkin et al.*, 1997]. For all UNE, teleseismically determined origin times are available from multiple sources, such as the International Seismological Centre (ISC) and *Thurber et al.* [2001].

[8] The Balapan test site region is divided by the ESE striking Chinrau fault (Figure 1). The southwestern subregion is covered by crystalline rocks, while the northeastern subregion is covered by alluvium [*Ringdal et al.*, 1992].

Bonner et al. [2001] reported that the shallow shear velocities of the SW subregion vary between about 2.45 km/s near the surface and 3.3 km/s at a depth of 2.5 km. Near-surface shear velocities in the NE subregion are about 0.4 km/s lower than in the SW subregion. At depths greater than about 1.5 km the difference in shear velocities in the two subregions tends to disappear. The regionally averaged P and S wave velocities are typical of the shields in much of the crust and reach about 8.0 and 4.7 km/s in the uppermost mantle, respectively [*Quin and Thurber*, 1992]. Paths from the test site to station BRV traverse a region covered by Precambrian and early Palaeozoic rocks. This region is flanked to the northeast by the West Siberian Basin [*Levashova et al.*, 2003]. A detailed description of the tectonics and geology of East Kazakhstan is given by *Ringdal et al.* [1992] and *Levashova et al.* [2003].

3. F-K Analysis

[9] Under the reciprocity theorem [*Aki and Richards*, 1980], velocity seismograms recorded at a station from many similar buried sources are identical to fictitious strain wave seismograms recorded at the source locations, generated by single forces acting upon the station location. The mathematical expression of the theorem was given for double-couple sources by *Spudich and Bostwick* [1987] and for dipole sources by *Nowack and Chen* [1999]. Using this theorem, we can treat the regional seismograms from Balapan explosions recorded at station BRV as seismograms from single forces at BRV, recorded at an array of strain meters located at the explosion locations.

[10] In the reciprocal recording geometry we can apply a conventional frequency–wave number (F-K) analysis technique to study the slownesses (or phase velocities) of the wavelets arriving at the source array. In the original (true) geometry the analysis yields the phase composition of the wavelets leaving the explosion sources (see Figure 1 of *Spudich and Bostwick* [1987] for an illustration on the equivalence between original and reciprocal recording ge-

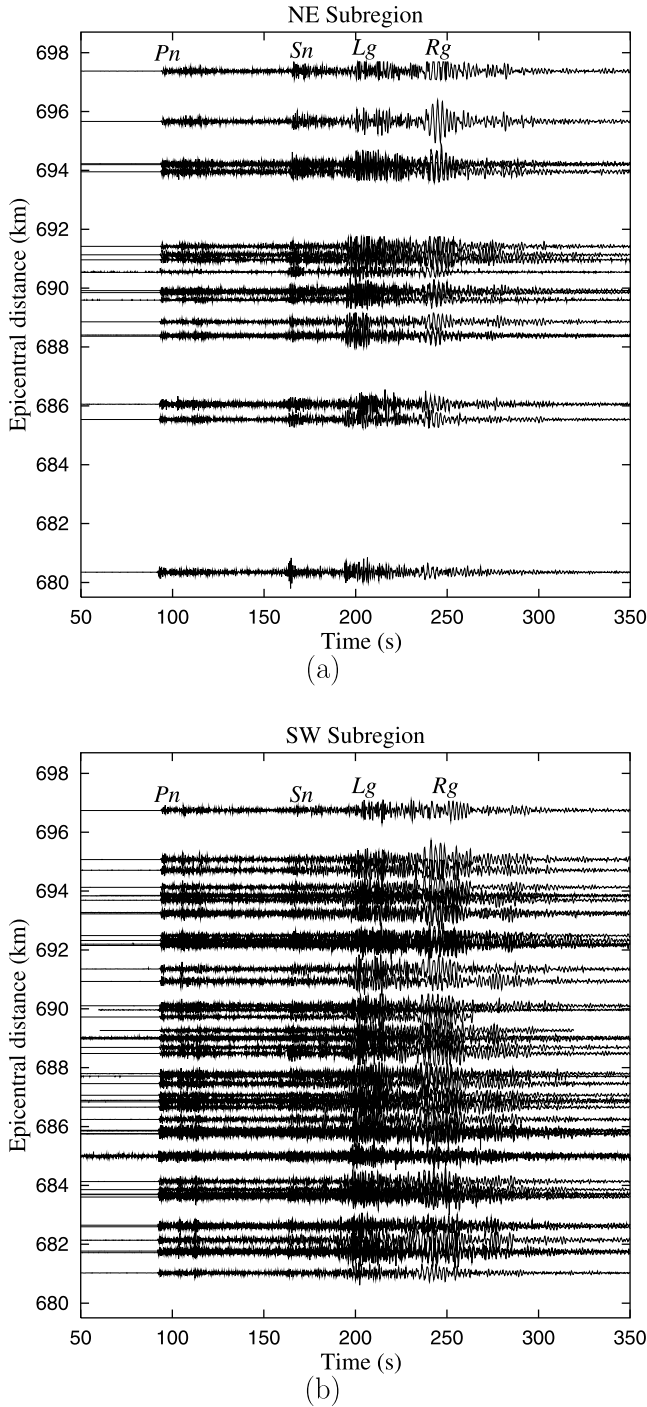


Figure 2. Raw record sections of 67 Balapan explosions used in this study: (a) 18 events in the slower velocity NE subregion and (b) 49 events in the faster velocity SW subregion. The record sections are aligned on the P_n travel time curve estimated from the ground truth origin times. Strong impulsive S_n waves are observed in the NE subsite, while the S_n in the SW subsite is rather weak.

ometries). The slowness power spectrum (P_c) at angular frequency ω and wave number \mathbf{k} ($=\omega\mathbf{s}$, where \mathbf{s} is the slowness vector) is determined by

$$P_c(\omega\mathbf{s}, \omega) = |U(\omega\mathbf{s}, \omega)|^2, \quad (1)$$

where U is the double Fourier transform of the waveforms $u(\mathbf{r}, t)$ recorded at location \mathbf{r} in the reciprocal geometry:

$$U(\omega\mathbf{s}, \omega) = \int_{-\infty}^{\infty} \sum_{j=1}^M u(\mathbf{r}_j, t) \exp[i(\omega\mathbf{s} \cdot \mathbf{r}_j - \omega t)] dt \quad (2)$$

and M is the number of time records.

[11] When a seismic wave is approximately nondispersive in a finite frequency range, coherent power spectral features can be enhanced by stacking the $P_c(\omega\mathbf{s}, \omega)$ over frequencies (ω) [Spudich and Bostwick, 1987]:

$$P_W(\mathbf{s}) = \frac{1}{N} \sum_{j=1}^N P_c(\omega_j\mathbf{s}, \omega_j) / m_j, \quad (3)$$

where N is the number of discrete frequencies, ω_j is the j th angular frequency, P_W is the stacked slowness power spectrum, and m_j is a normalization (whitening) factor given by

$$m_j = \max[P_c(\omega_j\mathbf{s}, \omega_j)]. \quad (4)$$

P_W indicates the relative strength of a plane wave leaving the source region in a finite frequency range. The prewhitening normalization applied through equations (3) and (4) removes the effect of nonflat responses of the instrument and wave propagation [Spudich and Bostwick, 1987] which are virtually the same for all records.

4. Source Depths

[12] Ground truth information on the depths and origin times of most Balapan UNE is not available. To estimate the depths of the UNE used in this study, we calibrate the scalings among the body wave magnitudes (m_b), the yields in kilotons (Y), and the depths in meters (H) of those Balapan UNE whose ground truth depths and/or yields are available. These scalings are then used to estimate H values of all other events from their m_b values. Several authors [e.g., Spivak, 1996; Bocharov *et al.*, 1989; V. Khalturin, personal communication, 2004] provided Y and m_b values for 19 Balapan explosions. The magnitudes (m_b) of Balapan nuclear explosions are given by Marshall *et al.* [1985] and Kim *et al.* [2001]. Using these values, we obtain a relationship (Figure 3)

$$m_b = 0.753 \log(Y) + 4.428. \quad (5)$$

[13] This relationship is very similar to that obtained by Ringdal *et al.* [1992].

[14] An empirical cube root rule of depth of burial in the Balapan test site is assumed (V. Khalturin, personal communication, 2004) [also cf. Lay *et al.*, 1984]:

$$H = c \cdot \sqrt[3]{Y}, \quad (6)$$

where H is the depth of burial in meters and c is a constant. The scaling relationship between m_b and H can be derived from equations (5) and (6):

$$m_b = a \log(H) + b, \quad (7)$$

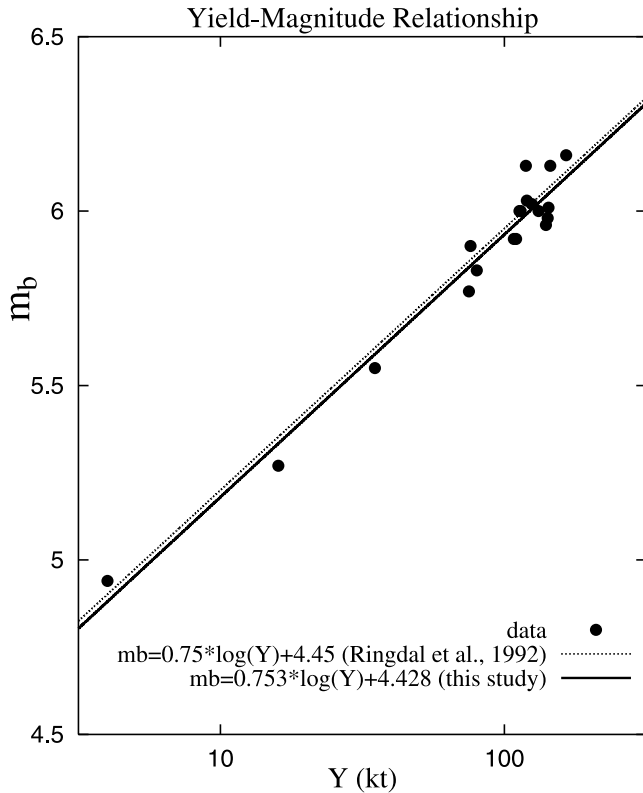


Figure 3. A linear relationship between yield (Y) and body wave magnitude (m_b) obtained in this study. The refined relationship is very close to the previous result of Ringdal *et al.* [1992].

where parameter a can be estimated to be 2.25 using equation (5) and the depth of burial rule and b is an unknown parameter that is directly related to c in equation (6). We use available ground truth values of H for 10 Balapan explosions in a linear regression with a fixed at 2.259 and estimate b to be -0.129 :

$$m_b = 2.259 \log(H) - 0.129. \quad (8)$$

[15] From the m_b - H relationship (8) we calculate the unknown depths of burial. Since the determined depths of burial are the relative distances from the surface, the absolute vertical location of the explosion is obtained by taking into account the surface topography (GTOPO30, compiled by the U.S. Geological Survey). The estimated depths have an average of 405 m, or ~ 120 m below sea level. The range of the depth variation from the average depth, as measured by the standard deviation, is 107 m. This range is much smaller than the lateral spread (epicentral span) of 17 km for the sources. This intuitively suggests that the source array in this study cannot resolve the vertical component of the slowness owing to the lack of vertical sampling (aliasing).

[16] When we assume alternative quarter root scaling of burial ($H = c\sqrt[4]{Y}$), the m_b - H relationship is estimated to be

$$m_b = 3.012 \log(H) - 2.147. \quad (9)$$

Under this scaling rule the depths of burial of the events used in this study are estimated to be between 202 and 642 m. The estimated depths of burial from the quarter root scaling rule display changes between -45 and 51 m relative to those obtained from the cube root scaling. The average absolute difference between the two sets of depths is 20 m. The variation in depths with change of the H - Y scaling rule is very small considering the distances from events to the station (around 690 km). Thus the effects of uncertainties in the estimated depths of burial should be trivial for the study. We use the depths determined from a cube root rule in equation (8) as reference values in this study.

[17] Scherbaum *et al.* [1991, equation (3)] give a quantitative relationship among the mean interstation distance within a source array, the slowness to be imaged, and the minimum frequency at which aliasing does not occur. Using that relationship with the measured vertical spacing of events (107 m) and the maximum source zone vertical slowness of 0.40 s/km [Bonner *et al.*, 2001], we estimate the minimum frequency for resolving vertical slowness to be 5.8 Hz. This frequency is higher than the Nyquist frequency of 5.2 Hz for one channel (s06Z) of the data. Therefore throughout this study we only analyze the horizontal slowness, or phase velocity, of the regional waves.

5. Adjustment of Origin Times

[18] As discussed in section 2, the event origin times are originally estimated using teleseismic body waves. For regional wave studies these origin times should be adjusted to improve their accuracy. In this study we adjust the origin times by aligning the P_n waveforms along a calibrated travel time curve. To do so, we first estimate the P_n travel time curve from Balapan to station BRV using the ground truth origin times of Balapan explosions reported by Adushkin *et al.* [1997].

[19] Eight of the 10 events with ground truth times belong to the data set of this study. We estimate the P_n arrival times of the 8 events by waveform cross correlation [Xie *et al.*, 1997] and determine the P_n travel time curve by linear regression as

$$L = 7.835T - 37.210, \quad 680 \text{ km} < L < 698 \text{ km}, \quad (10)$$

where L is the epicentral distance and T is the travel time. We then align the P_n waveforms from all events to the calibrated travel time curve in equation (10) by adjusting the event origin times.

[20] Figure 2 shows the raw records after they are aligned to the P_n travel time curve. The adjustments to the teleseismically estimated origin times by the ISC and Thurber *et al.* [2001] are mostly less than 0.03 s and always less than 0.09 s. We find that using these adjustments (also known as “source statics” [cf. Spudich and Bostwick, 1987; Xie *et al.*, 1996]) enhances the resolution of coherent phase composition in the slowness power spectral analysis.

6. Results

6.1. General Features

[21] The approximate frequency range in which effects of spatial aliasing and location errors can be suppressed is

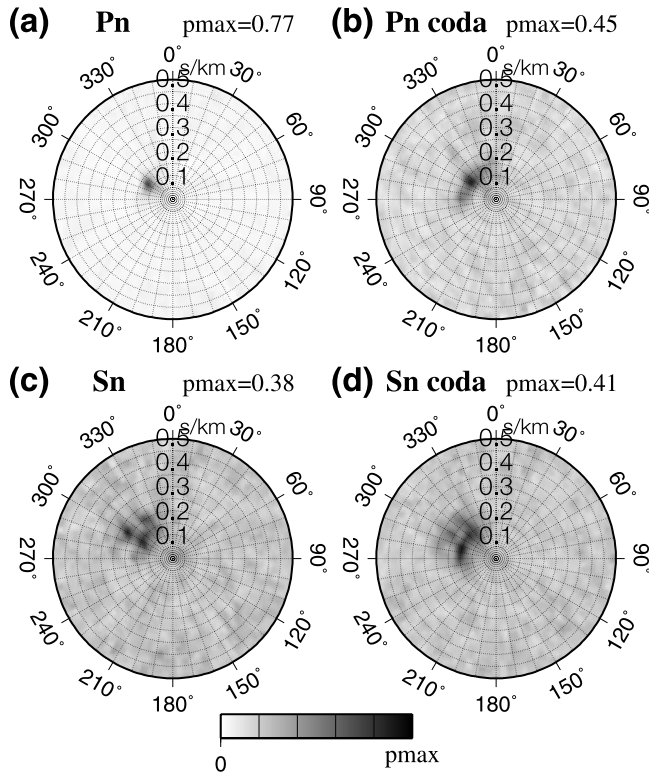


Figure 4. Slowness power spectra of (a) Pn , (b) Pn coda, (c) Sn , and (d) Sn coda. The event lapse time windows for Pn , Pn coda, Sn , and Sn coda are 92 to 96 s, 125 to 130 s, 162 to 170 s, and 178 to 186 s, respectively. The frequency band used is 0.5 to 3.0 Hz. Notation “pmax” indicates the maximum power spectrum. The slowness power spectra of Pn and Sn coda are similar to those of the primary Pn and Sn . The wider azimuthal spread of coda spectra indicates slightly different takeoff angles associated with near-source scattering. See color version of this figure in the HTML.

given by *Spudich and Bostwick* [1987] and *Scherbaum et al.* [1991] [also cf. *Xie et al.*, 1996, equation (3)]:

$$\frac{N}{4 \sum_{i,j=1}^N (\mathbf{x}_i - \mathbf{x}_j) \cdot \mathbf{s}} \leq f \leq \frac{v}{4\delta r}, \quad (11)$$

where N is the number of events, v is the source zone velocity, \mathbf{x}_i is the location of the i th event, \mathbf{s} is the slowness vector, and δr is the magnitude of the location uncertainty. In this analysis, only phase velocity is analyzed; thus v refers to phase velocity. Assuming a near-source v of 2.5 km/s [Bonner et al., 2001], typical mislocation (δr) of 0.2 km, and using the average intersource distance of 10.87 km among the UNE used, we have

$$0.05 \text{ Hz} \leq f \leq 3.12 \text{ Hz}. \quad (12)$$

[22] Considering also the instrument roll-off at lower frequencies, we use a frequency band between 0.5 and 3.0 Hz throughout the slowness (phase velocity) power spectral analysis unless otherwise specified. The slowness power spectral analysis is made on a finely gridded slowness azimuth domain with discrete slowness interval of

0.005 s/km and discrete azimuthal interval of 1° . Thus the uncertainties introduced by the discrete grid system are ± 0.0025 s/km and $\pm 0.5^\circ$. This corresponds to a velocity uncertainty of ± 0.17 km/s for 8.0 km/s and ± 0.05 km/s for 4.0 km/s. The uncertainty is reduced drastically with decreasing phase velocity. Thus slower phase velocities can be determined with a high precision.

[23] In Figure 4 a the slowness power spectrum of Pn waves has a maximum value at horizontal slowness (s_h) of 0.125 s/km, which corresponds to P waves travelling in the uppermost mantle with a phase velocity (v_h) of 8.0 km/s [Quin and Thurber, 1992]. The azimuth of the maximum power is 303° which agrees with the great circle azimuths of events ($302.2^\circ - 304.5^\circ$). The notation “pmax” in Figure 4 a indicates the maximum coherency of the slowness power spectra, which varies between 0 and 1. Thus it directly represents the magnitude of coherent phases in the given record section. The Pn phase velocity from F-K analysis (8.0 km/s) shows a difference of 0.165 km/s to that from the ground truth origin times (7.835 km/s) in equation (10). The difference is caused by the introduction of discrete slowness angle domain in the F-K analysis. The difference resides within the expected uncertainty range (± 0.17 km/s).

[24] The slowness power spectrum of the expected Sn window, which spans group velocities between about 4.0 and 4.3 km/s, exhibits two dominant phases with s_h of 0.14 and 0.205 s/km, respectively (Figure 4c). The phase with an s_h of 0.14 s/km ($v_h = 7.1$ km/s) spreads into multiple azimuths, implying that it is composed of multiple forward scattered lower crustal (Pg) waves. The phase with an s_h of 0.205 s/km ($v_h = 4.8$ km/s) is the shear wave propagating in the uppermost mantle. The scattered Pg phase displays a comparable energy level to the Sn phase (Figure 5). This implies that a strong lateral velocity heterogeneity or topography variation must be present along the Pg ray path in the near-source region. The complexity of the Sn phase is discussed more in section 6.2.

[25] The phase velocities of Pn and Sn coda are similar to those of Pn and Sn (Figure 4). However, the azimuthal distributions of the maximum slowness power spectra of the coda are wider than those of Pn and Sn (Figure 4). This indicates that the waves constituting the coda tend to undergo forward scattering in the near-source region. The azimuthal span of slowness power spectra of coda increases with time, indicating that the scattered rays tend to increas-

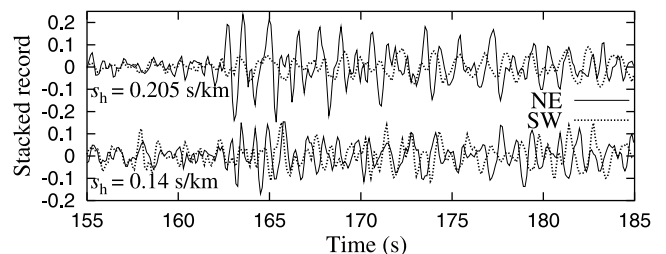


Figure 5. Slant-stacked seismograms of Sn window along horizontal slowness (s_h) of 0.205 and 0.14 s/km that are two dominant phases in the window. The stronger Sn at the NE subsite is mainly caused by enhancement of the phase with an s_h of 0.205 s/km.

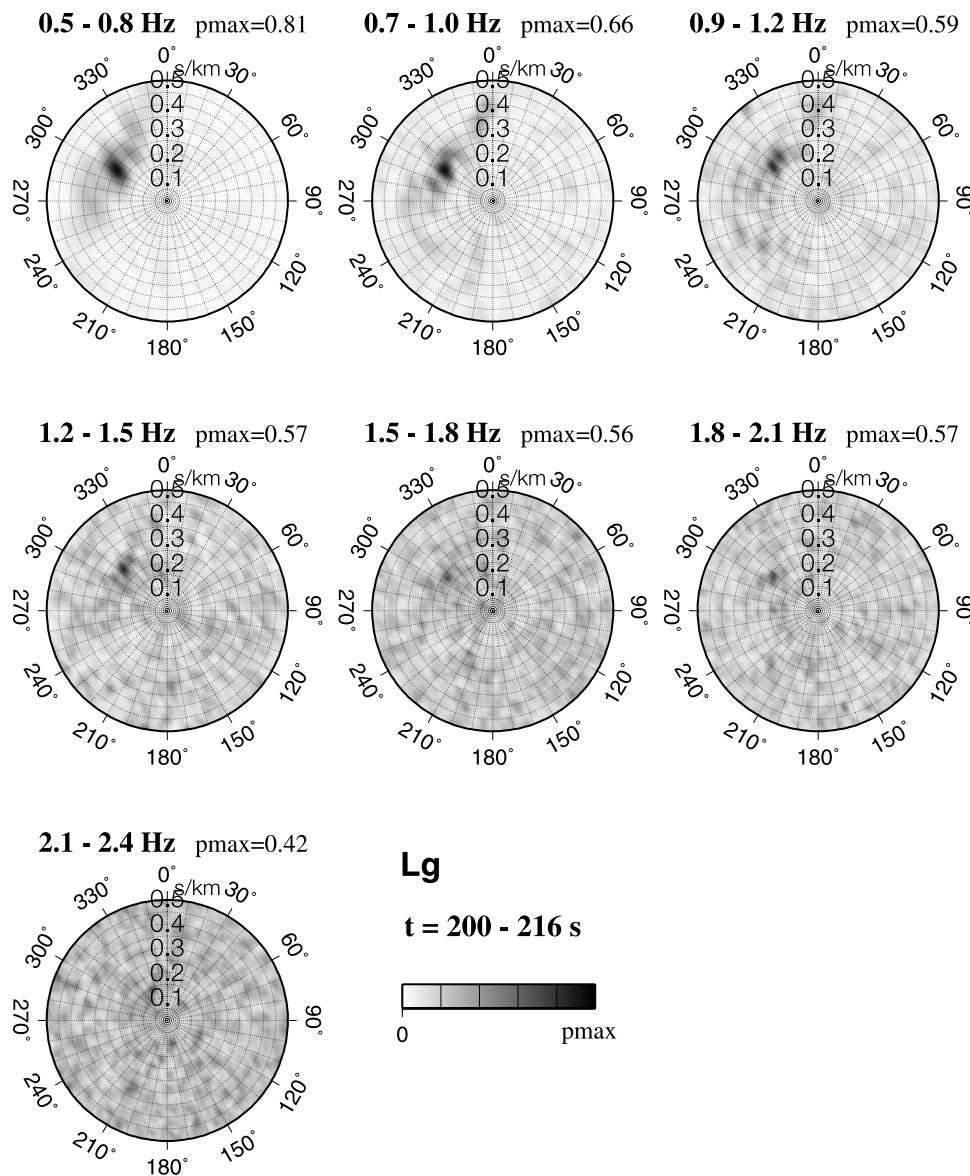


Figure 6. Slowness power spectra of the Lg window in various frequency bands. The dominant phase with phase velocity of 4.2 km/s is observed in a frequency range between 0.5 and 2.0 Hz, above which the coherency in slowness power spectra degrades. See color version of this figure in the HTML.

ingly deviate from the great circle azimuth toward later coda.

[26] The Lg waves are composed of crust-guided shear waves, with group velocity of 3.0 to 3.6 km/s [e.g., Kennett, 2002]. The dominant phase in the expected Lg window has a v_h of 4.2 km/s at frequencies up to 2.0 Hz (Figure 6). This phase velocity is typical of Lg observed in conventional receiver array analysis [e.g., Der et al., 1984]. The coherency of the phase in the Lg window degrades at frequencies above 2.0 Hz.

[27] It was reported that source spectral shapes tend to change with the sizes (event magnitudes) of the UNE [Xie, 2002]. We examine the influence of the source spectral change with event size in the slowness power spectra in the following empirical way. For every event we first estimate the shape of the Lg source spectrum using the source model and source scalings among event magnitude, mo-

ment, and corner frequencies developed by Xie [2002]. We then deconvolve the estimated Lg source spectra from the observed Lg spectra and recompute the slowness power spectra. The result is compared with that obtained without this deconvolution.

[28] Figure 7 shows the slowness power spectra of an Lg wave with the source spectral correction. The slowness power spectra are very similar to those without source spectral correction shown in Figure 6. This is probably because the magnitudes of the analyzed explosion data are distributed in a narrow range of magnitude between 4.8 and 6.2, with a majority (87%) of the events having magnitudes larger than 5.5. The source spectral variation with the magnitudes is not significant in this analysis.

[29] In a time window where a fundamental mode Rayleigh (Rg) wave is expected, the dominant signal frequency is around 0.2 to 0.8 Hz. We note that as the

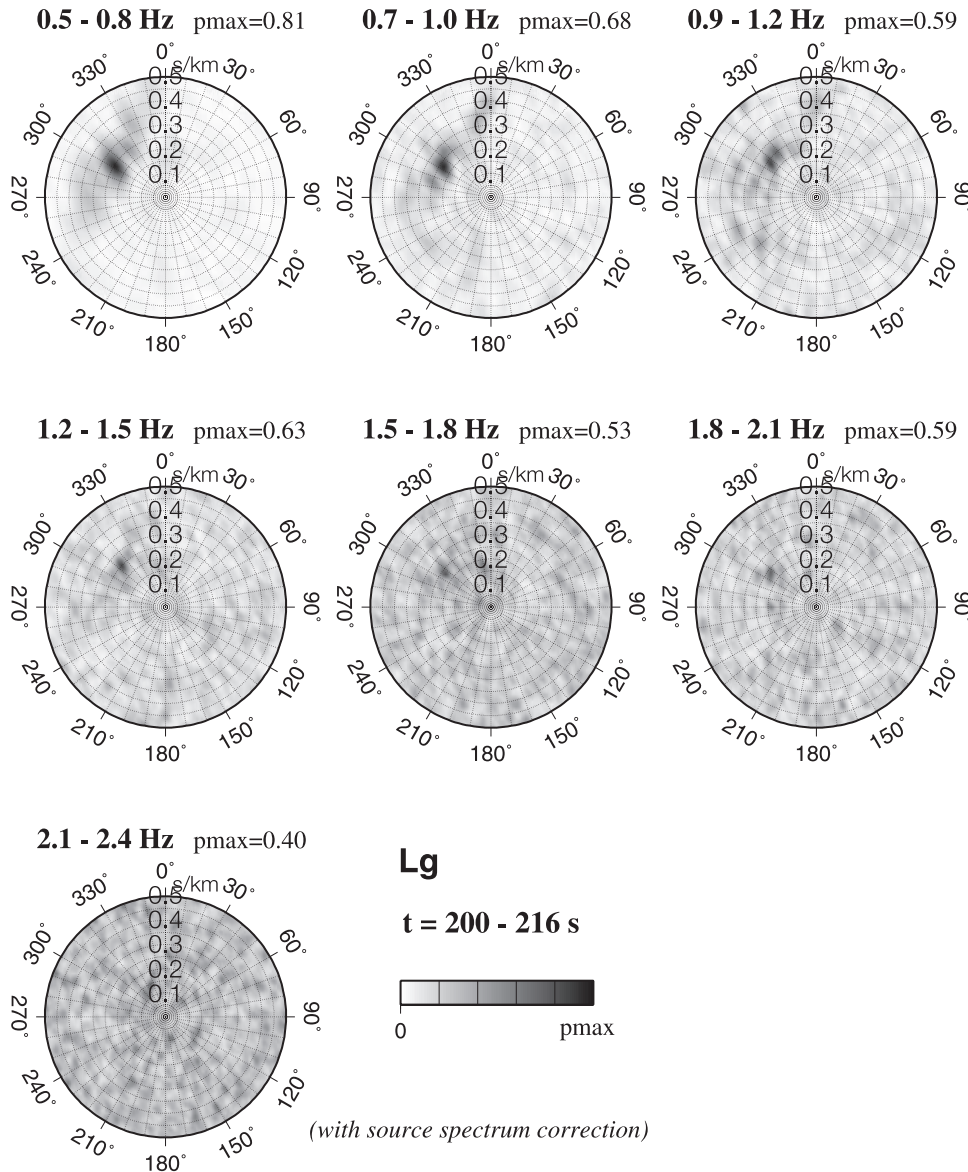


Figure 7. Slowness power spectra of the Lg window with source spectral shape correction considering event magnitude and source corner frequency [Xie, 2002]. No significant change is found between the results presented here and those in Figure 6. See color version of this figure in the HTML.

short-period instruments of BRV used in this study (channels s06Z and sZ01) have steep high-pass filtering below 0.4 Hz, the energy in the low-frequency range (<0.4 Hz) is underestimated relative to that in the high-frequency range. In this study we constrain the analysis to the higher-frequency range ($f > 0.4$ Hz) at which normally regional Lg energy is dominant. The dominant phase velocity in that window is 3.0 km/s at frequencies between 0.5 and 0.8 Hz and appears to increase gradually with frequency (Figure 8); it reaches 4.0 km/s at frequencies between 0.9 and 1.2 Hz and 5.7 km/s at frequencies between 1.3 and 1.6 Hz. At frequencies above 1.6 Hz the coherency in the slowness power spectra decreases drastically owing to a lack of coherent high-frequency energy. These observed high phase velocities ($v_h \geq 4.0$ km/s) at frequencies higher than 0.8 Hz are too high for the Rg wave. These high phase velocities suggest that the Rg wave is attenuated out at these high

frequencies, leaving the dominant signals to be those from forward scattered higher mode or mantle S waves. To confirm that the Rg is absent at higher frequencies, we conduct multiple filter analysis on signals in the expected Rg window using computer programs of Herrmann [2002]. The result clearly indicates that the coherent dispersive fundamental mode Rayleigh wave is only observed in the frequency range between about 0.2 and 0.8 Hz (Figure 9).

[30] In Figure 10 we show records at four locations (events A, B, C, D) with epicentral distances of about 695 and 681 km. The four locations are marked on the map in Figure 1b. The selected pairs of records are from events with similar magnitudes (m_b): The m_b of events A and B are 6.01 and 5.86 and those of events C and D are 5.29 and 5.45, respectively. The variation of Rg amplitudes with m_b is obvious in Figure 10. It is well known that the strength of Rg is dependent on both the size of explosion (m_b) and the

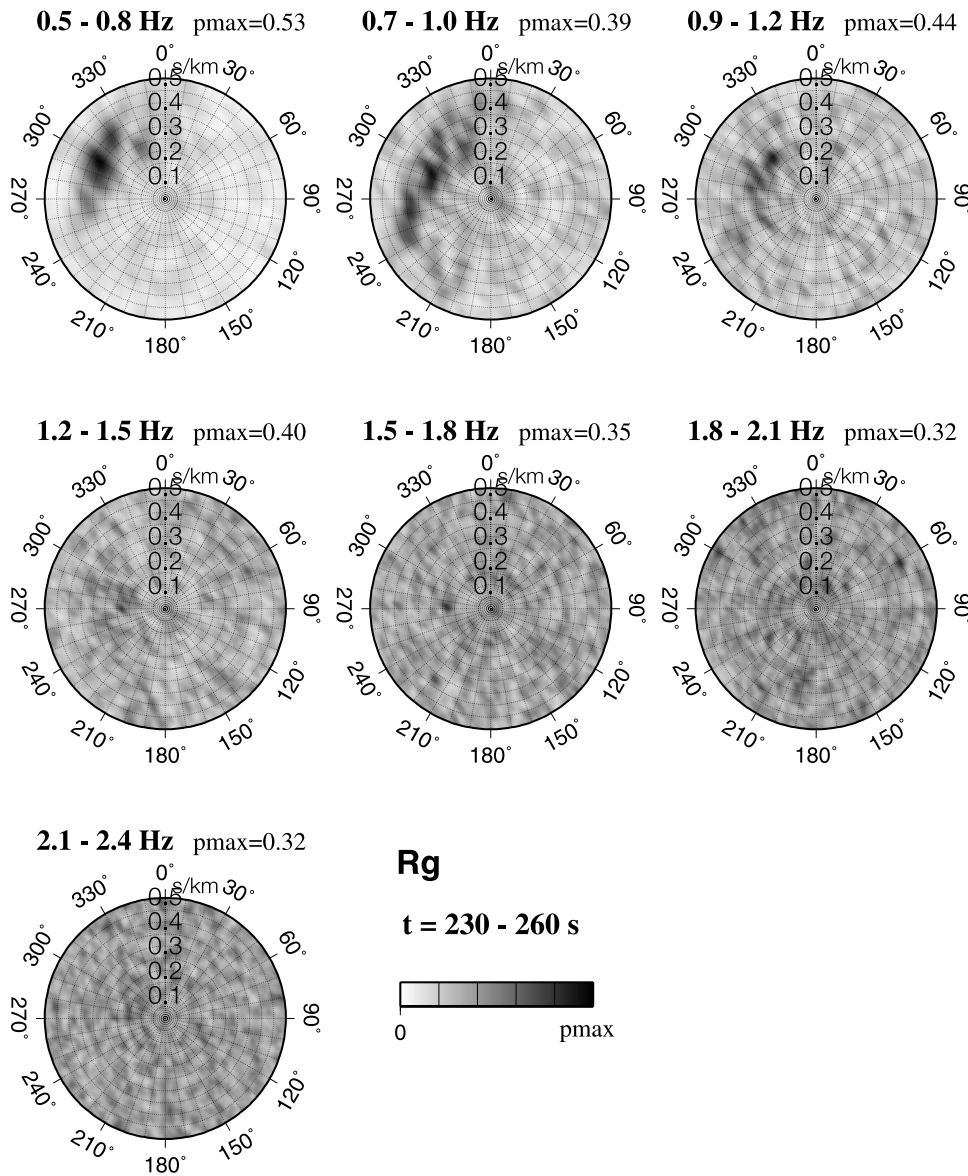


Figure 8. Slowness power spectra of the expected R_g window for various frequencies. The phase velocity of R_g is 3.0 km/s at frequencies between 0.5 and 0.8 Hz, which is the dominant frequency range of coherent R_g signal. Phases at higher frequencies appear to be scattered L_g and body waves with higher phase velocities. Note the coherency generally degrades with frequency. See color version of this figure in the HTML.

depth of burial. In Figure 10, on the other hand, the L_g amplitudes are less variable than the R_g amplitudes.

[31] The slowness power spectra of L_g and R_g allow us to explore whether or not the L_g phase is excited by a source zone R_g scattering. In a hypothesis that R_g -to- S scattering is primarily responsible for the L_g excitation the scattering process ought to cause phase shift of the observed L_g such that the observed spectral power spectrum would be dominated by one or multiple wavelets with phase velocities distinctly different from that of the SmS . One peak in the slowness power spectrum at the R_g slowness is expected if the scattered R_g exists in the near-source region as a single planar wavelet. Multiple peaks are expected if R_g exists as a single spherical wavelet or as multiple wavelets. This hypothesis can now be tested.

[32] We observe that the L_g slowness power spectra are dominated by a phase with a v_h of 4.2 km/s at frequencies between 0.5 and 2.0 Hz, while the phase composition in the R_g window varies with frequency. A coherent and dispersive fundamental mode Rayleigh wave with v_h of 3.0 km/s is observed below 0.8 Hz (Figures 8 and 9). The fundamental mode Rayleigh wave is not observed at high frequencies (>0.8 Hz) since it is attenuated out during the regional distance (around 690 km) propagation. However, for any normally dispersed Rayleigh wave it is required that its phase velocity decrease with frequency. Therefore we expect the phase velocity of a Rayleigh wave to be slower than 3.0 km/s at frequencies above 0.8 Hz. Since the observed dominant L_g phase velocity at frequencies between 0.5 and 2.0 Hz (particularly, above 0.8 Hz) is

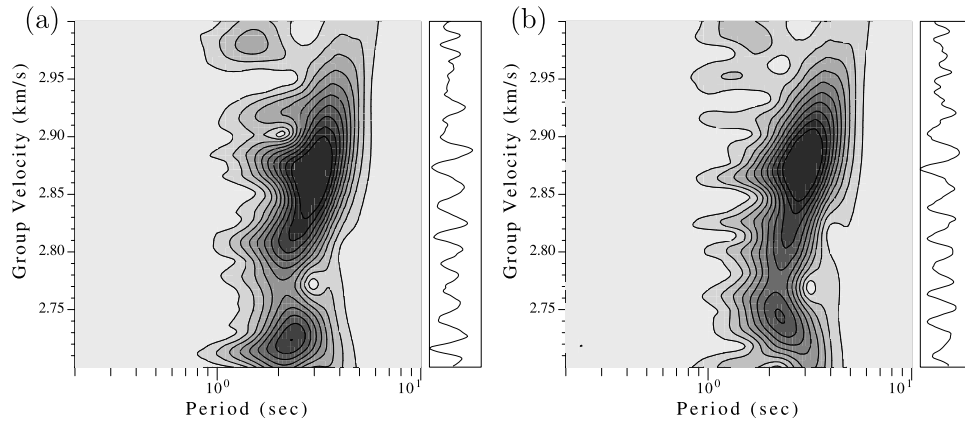


Figure 9. Examples of multiple filter analysis of *Rg* signals, conducted for two nuclear explosion data of (a) 3 April 1988 and (b) 22 January 1989. The *Rg* energy is concentrated in the period range between 2 and 5 s. All *Rg* records of this study have frequency contents that are very similar to the two examples presented.

4.2 km/s (which is much higher than 3.0 km/s), the *Lg* has a faster phase velocity than *Rg* at these frequencies. The strong coherent peaks observed in the *Lg* and *Rg* slowness power spectra and the difference in their phase velocities do not agree with the hypothesis of a dominant *Rg*-to-*Lg* scattering. Therefore *Rg*-to-*Lg* scattering does not appear to be a dominant mechanism for *Lg* excitation by the Balapan UNE. However, this observation does not rule out the possible existence of a weaker *Rg*-to-*S* scattering in the source region. Such a scattering may exist, but the strengths of scattered *Rg* wavelets should be significantly lower than are those of the *SmS* type of wavelets which dominate the *Lg* slowness power spectrum.

6.2. Effect of Source Site Geology on Shear Waves

[33] To investigate the influence of local geology on the phase composition of regional waves from nuclear explosions, we split the data set into two subgroups according to

event locations and local geology (Figure 1b). The explosions are well separated into the two regions by the dashed line in Figure 1b which approximately delineates the boundary of two adjacent velocity structures in the Balapan region. The shear wave velocity of the uppermost crust at the NE subregion is about 0.4 km/s lower than the SW subregion [Bonner *et al.*, 2001].

[34] We find that the phase compositions from the two subgrouped data exhibit a clear difference in the expected *Sn* window (Figure 11). The slowness power spectrum for the slower velocity NE subregion is dominated by a strong shear wave energy with an s_h of 0.205 s/km. On the other hand, shear wave energy is relatively weak for the higher-velocity SW subregion. In Figure 10 we compare the raw seismograms from the two subregions. A striking feature is that the records from the NE subregion have strong and impulsive *Sn* waves, while those from the SW region have weak *Sn* waves (see also Figure 2).

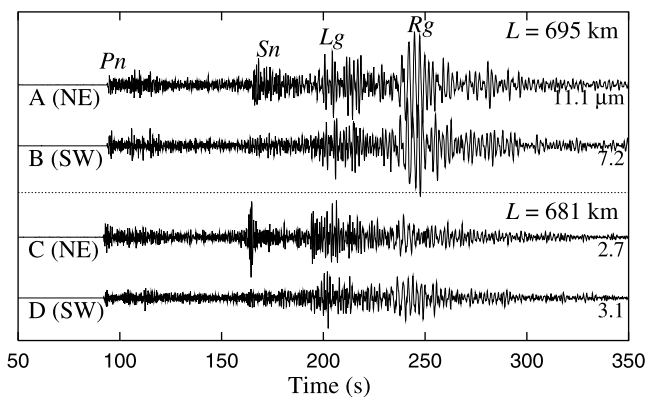


Figure 10. BRV seismograms from four events (A, B, C, D) in Figure 1b. The seismograms are normalized for *Lg* waves. The reference *Lg* amplitudes for normalization are presented at the ends of records. Strong *Sn* waves are observed in the seismograms from the NE subsite that have a slower velocity structure, while the *Sn* waves are rather weak in the records from the SW subsite with a faster velocity structure.

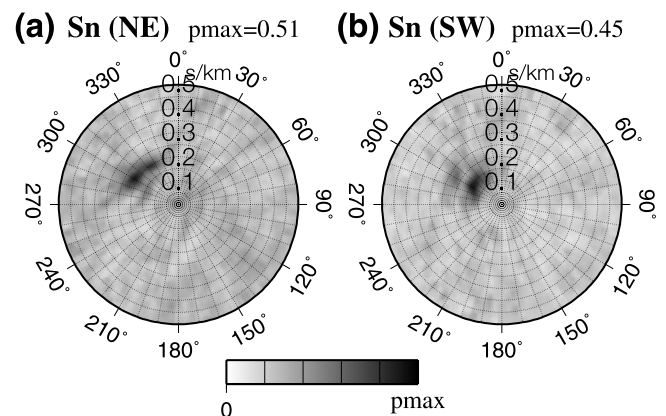


Figure 11. Slowness power spectra of the expected *Sn* window for data sets from two subsites ((a) NE, (b) SW) which were divided according to the velocity structure. The NE subsite has a lower-velocity structure than the SW subsite. The *Sn* window used is between 162 and 170 s. The frequency band used is 0.5 to 3.0 Hz. See color version of this figure in the HTML.

[35] We also examine the relative amplitudes of shear wave and scattered Pg waves using a slant stack technique [e.g., Kanasewich, 1981]. We stack the waveforms in the expected Sn window along the two dominant slownesses (s_h) of 0.14 and 0.205 s/km (Figure 5). The stacked records show that the strong Sn energy from the NE subsite is largely caused by the larger amplitudes of the mantle shear wave propagating with an s_h of 0.205 s/km. On the other hand, the amplitude of the shear wave from the SW subsite is weaker as it becomes comparable to that of the scattered Pg wave with an s_h of 0.14 s/km.

[36] The amplitude of the Lg waves is less variable with the source locations than is that of the Sn , as shown in Figure 10. At first glance this is somewhat puzzling because both Lg and Sn waves are regional shear waves, probably having similar takeoff angles when they leave the sources. A detailed examination of the Fourier spectral amplitudes of Lg and Sn (not shown) reveals that their frequency contents are different at station BRV. The spectra of Sn are enriched between about 1 and 3 Hz as compared to Lg spectra. Apparent corner frequencies of Sn are 2 to 3 times higher than are those of Lg . This is consistent with the substantial report of Xie [2002] that different regional waves exhibit different source corner frequencies from UNE.

[37] Our observation that Sn has both an enriched high-frequency content and a more variable amplitude than that of Lg is intriguing. It suggests that the efficiency of shear wave excitation by UNE may be dependent on source site geology in a frequency variable manner: Shear wave excitation may be more variable at higher frequencies. This scenario is consistent with a physical consideration that the excitation of shear waves with shorter wavelengths is more affected by the shallow source zone geological structures.

7. Conclusions and Discussion

[38] There are several proposed mechanisms for regional shear wave generation by underground nuclear explosions (UNE). However, many aspects, such as their relative contributions to the regional shear wave development, remain unclear. To understand the origin of the shear waves, it is necessary to explore the composition of the shear wave field in the near-source region. We could investigate the near-source phase composition of regional seismic waves leaving UNE at the Balapan test site by applying a slowness power spectral analysis to the source array under the reciprocity theorem. The dominant Pn phase velocity (v_h) is about 8.0 km/s. The energy in the expected Sn window is composed of scattered crustal Pg waves with a v_h of 7.1 km/s and mantle shear waves with a v_h of 4.8 km/s. The Lg wave in a frequency range between 0.5 and 2.0 Hz has a phase velocity of 4.2 km/s that is typical for supercritically reflected crustal S waves. On the other hand, the expected Rg window is dominated by a fundamental Rayleigh wave with a v_h of 3.0 km at frequencies below 0.8 Hz. Above 0.8 Hz the phase coherency degrades drastically owing to a strong attenuation of Rayleigh waves during propagation. Thus Rayleigh wave phase velocity is not measurable at these higher frequencies.

[39] However, a normal surface wave dispersion requires that Rayleigh (Rg) wave phase velocity at higher frequencies be slower than 3.0 km/s. Consequently, if the Lg wave

between 0.5 to 2.0 Hz were dominantly generated by Rg wave scattering, one would expect the Lg phase velocity in the near-source region to be that of Rg . If the scattered Rg is composed of a plane wave in the near-source region, it is expected to display a strong peak with a phase velocity of Rg in the slowness power spectrum. On the other hand, if the scattered Rg consists of either a nonplanar (spherical) wave or multiple wavelets, multiple peaks are expected in the slowness power spectrum. None of these expectations were observed in the F-K analysis. On the contrary, our observation displays a faster SmS -type phase velocity of 4.2 km/s. We therefore infer that the Rg -to- S scattering does not appear to be a dominant mechanism for Lg wave generation by the Balapan explosions. However, this observation does not rule out the possible existence of a secondary Rg -to- S scattering because the slowness power spectrum reflects the most dominant phase composition. A similar inference can be made for the Sn wave excitation based on its faster phase velocities. With this observation alone it is still difficult to identify the most influential source of shear wave generation from UNE among the other previously presented mechanisms. More information on, for instance, the delay time of spalling, the topography change by spalling, and rock fracturing by shock waves, etc., needs to be incorporated to constrain the dominant mechanisms.

[40] The geology of the source region appears to play an important role on the strength of mantle shear wave in the expected Sn window. In that window, slower near-surface velocity in the source region seems to enhance shear waves. On the other hand, the strength of Lg waves is much more robust with varying source region geology. The Lg window generally contains lower-frequency content relative to the Sn window. Typically, for the Balapan nuclear explosions used in this study the apparent corner frequencies are near 1 Hz for Lg and about 3 Hz for Sn . Therefore our observation implies that source region geology tends to have a stronger influence on the strength of higher-frequency shear waves. More observational and simulation work may be needed to understand and confirm this phenomenon.

[41] **Acknowledgments.** We thank Howard Patton, Paul Richards, and Bill Menke for fruitful comments on the study; Won-Young Kim for information on data and instrument response; Vitaly Khalturin for information on nuclear explosions at Kazakhstan; and Cliff Thurber for computation of calibrated origin time with refined depth values. The paper benefited from fruitful review comments by Howard Patton, an anonymous reviewer, and an Associate Editor. We are grateful to Bob Herrmann for making his code available which was used in the multiple filter analysis. The work was supported by DOE grant DE-FC52-03NA99514. This is Lamont-Doherty Earth Observatory contribution 6817.

References

- Adushkin, V. V., V. A. An, V. M. Ovchinnikov, and D. N. Krasnoshechekov (1997), A jump of the density on the outer-inner core boundary from the observations of PKiKP waves on the distance about 6 degrees (in Russian), *Dokl. Akad. Nauk*, 354(3), 382–385.
- Aki, K., and P. G. Richards (1980), *Quantitative Seismology, Theory and Methods*, vol. 1, W. H. Freeman, New York.
- Bocharov, V. S., S. A. Zelentsov, and V. I. Mikhailov (1989), Characteristics of 96 underground nuclear explosions at the Semipalatinsk test site (in Russian), *At. Energ.*, 67, 210–214.
- Bonner, J. L., D. C. Pearson, W. S. Phillips, and S. R. Taylor (2001), Shallow velocity structure at the Shagan River test site in Kazakhstan, *Pure Appl. Geophys.*, 158, 2017–2039.
- Day, S. M., and K. L. McLaughlin (1991), Seismic source representations for spall, *Bull. Seismol. Soc. Am.*, 81, 191–201.
- Der, Z., M. E. Marshall, A. O'Donnell, and T. W. McElfresh (1984), Spatial coherence structure and attenuation of the Lg phase, site effects,

- and interpretation of the *Lg* coda, *Bull. Seismol. Soc. Am.*, *74*, 1125–1148.
- Gupta, I. N., C. S. Lynnes, T. W. McElfresh, and R. A. Wagner (1990), F-K analysis of NORESS array and single station data to identify sources of near-receiver and near-source scattering, *Bull. Seismol. Soc. Am.*, *80*, 2227–2241.
- Gupta, I. N., W. W. Chan, and R. A. Wagner (1992), A comparison of regional phases from underground nuclear explosions at east Kazakh and Nevada test sites, *Bull. Seismol. Soc. Am.*, *82*, 352–382.
- Gutowski, P. R., F. Hron, D. E. Wagner, and S. Treitel (1984), *S**, *Bull. Seismol. Soc. Am.*, *74*, 61–78.
- Herrmann, R. B. (2002), *Computer Programs in Seismology*, version 3.30, Saint Louis Univ., St. Louis, Mo.
- Kanasewich, E. R. (1981), *Time Sequence Analysis in Geophysics*, 3rd ed., Univ. of Alberta, Edmonton, Canada.
- Kennett, B. L. N. (2002), *The Seismic Wavefield*, vol. 2, *Interpretation of Seismograms on Regional and Global Scales*, Cambridge Univ. Press, New York.
- Kim, W.-Y., P. G. Richards, V. Adushkin, and V. Ovtchinnikov (2001), Borovoye digital seismogram archive for underground nuclear tests during 1966–1996, technical report, Lamont-Doherty Earth Obs. of Columbia Univ., Palisades, N. Y.
- Lay, T., D. V. Helmberger, and D. G. Harkrider (1984), Source models and yield-scaling relations for underground nuclear explosions at Amchitka Island, *Bull. Seismol. Soc. Am.*, *74*, 843–862.
- Levashova, N. M., K. E. Degtyarev, M. L. Bazhenov, A. Q. Collins, and R. Van der Voo (2003), Permian paleomagnetism of East Kazakhstan and the amalgamation of Eurasia, *Geophys. J. Int.*, *152*, 677–687.
- Marshall, P. D., T. C. Bache, and R. C. Lilwall (1985), Body wave magnitudes and locations of Soviet underground nuclear explosions at Semipalatinsk test site, *At. Weapons Res. Estab. Rep. O 16/84*, Her Majesty's Stn. Off., Norwich, U.K.
- Massé, R. P. (1981), Review of seismic source models for underground nuclear explosions, *Bull. Seismol. Soc. Am.*, *71*, 1249–1268.
- Myers, S. C., W. R. Walter, K. Mayeda, and L. Glenn (1999), Observations in support of *Rg* scattering as a source for explosion *S* waves: Regional and local recordings of the 1997 Kazakhstan depth of burial experiment, *Bull. Seismol. Soc. Am.*, *89*, 544–549.
- National Nuclear Centre of the Republic of Kazakhstan (1999), Proceedings of the Workshop on IMS Location Calibration, technical report, Oslo, Jan.
- Nowack, R., and W.-P. Chen (1999), Source-receiver reciprocity and empirical Green's functions from chemical blasts, *Bull. Seismol. Soc. Am.*, *89*, 538–543.
- Patton, H. J., and S. R. Taylor (1995), Analysis of *Lg* spectral ratios from NTS explosions: Implications for the source mechanisms of spall and the generation of *Lg* waves, *Bull. Seismol. Soc. Am.*, *85*, 220–236.
- Quin, H. R., and C. H. Thurber (1992), Seismic velocity structure and event relocation in Kazakhstan from secondary *P* phases, *Bull. Seismol. Soc. Am.*, *82*, 2494–2510.
- Ringdal, F., P. D. Marshall, and R. W. Alewine (1992), Seismic yield determination of Soviet underground nuclear explosions at the Shagan River test site, *Geophys. J. Int.*, *109*, 65–77.
- Scherbaum, F., D. Gilard, and N. Deichmann (1991), Slowness power analysis of the coda composition of two microearthquake clusters in northern Switzerland, *Phys. Earth Planet. Inter.*, *67*, 137–161.
- Spivak, A. A. (1996), Aftershocks of underground nuclear explosions (in Russian), *Geoecology*, no. 6, 27–42.
- Spudich, P., and T. Bostwick (1987), Studies of the seismic coda using an earthquake cluster as a deeply buried seismograph array, *J. Geophys. Res.*, *92*(B10), 10,526–10,546.
- Thurber, C., C. Trabant, F. Haslinger, and R. Hartog (2001), Nuclear explosion locations at the Balapan, Kazakhstan, nuclear test site: The effects of high-precision arrival times and three-dimensional structure, *Phys. Earth Planet. Inter.*, *123*, 283–301.
- Vogfjörd, K. S. (1997), Effects of explosion depth and Earth structure on the excitation of *Lg* waves: *S** revisited, *Bull. Seismol. Soc. Am.*, *87*, 1100–1114.
- Wallace, T., D. Helmberger, and G. Engen (1985), Evidence for tectonic release from underground nuclear explosions in long period *S* waves, *Bull. Seismol. Soc. Am.*, *75*, 157–174.
- Xie, J. (2002), Source scaling of *Pn* and *Lg* spectra and their ratios from explosions in central Asia: Implications for the identification of small seismic events at regional distances, *J. Geophys. Res.*, *107*(B7), 2128, doi:10.1029/2001JB000509.
- Xie, J., L. Cong, B. J. Mitchell, and J.-M. Chiu (1996), Complexities in high-frequency seismic waveforms due to three-dimensional structure in the New Madrid Seismic Zone, *J. Geophys. Res.*, *101*(B3), 5751–5778.
- Xie, J., Z. Liu, L. Cong, R. B. Herrmann, and J.-M. Chiu (1997), Rupture properties of clustered microearthquakes near intersecting intraplate faults of New Madrid Seismic Zone: Implications for fault weakening, *J. Geophys. Res.*, *102*(B4), 8187–8202.
- Xie, X.-B., and T. Lay (1994), The excitation of *Lg* waves by explosions: A finite-difference investigation, *Bull. Seismol. Soc. Am.*, *84*, 324–342.

T.-K. Hong and J. Xie, Lamont-Doherty Earth Observatory of Columbia University, 61 Route 9W, Palisades, NY 10964, USA. (tkhong@ldeo.columbia.edu; xie@ldeo.columbia.edu)